Chinese Chemical Letters 36 (2025) 109793

Contents lists available at ScienceDirect

Chinese Chemical Letters

journal homepage: www.elsevier.com/locate/cclet

Promoting the generation of active sites through "Co-O-Ru" electron transport bridges for efficient water splitting

Zuyou Song[1], Yong Jiang[1], Qiao Gou, Yini Mao, Yimin Jiang, Wei Shen, Ming Li, Rongxing He*

Key Laboratory of Luminescence Analysis and Molecular Sensing (Southwest University), Ministry of Education, College of Chemistry and Chemical Engineering, Southwest University, Chongqing 400715, China

ARTICLE INFO

Article history:
Received 19 January 2024
Revised 13 March 2024
Accepted 19 March 2024
Available online 20 March 2024

Keywords:
Heteroatom doping
Reconstruction
V leaching
Electron transfer
Overall water splitting

ABSTRACT

Exploring the intrinsic reasons for the dynamic reconstruction of catalysts during electrocatalytic reactions and their impact on activity enhancement still face severe challenges. Herein, the bifunctional catalyst Ru/V-CoO/CP with doping strategy and heterostructure was synthesized for overall water splitting. The Ru/V-CoO exhibits excellent activity for HER and OER with low overpotentials of 49, 147 mV at a current density of 10 mA/cm^2 in 1.0 mol/L KOH, respectively. The assembled electrolytic cell just needs voltages of 1.47 and 1.71 V to achieve 10 and 350 mA/cm^2 current density under the same conditions and delivers an outstanding stability for over 100 h, which is far superior to the commercial RuO_2||Pt/C cell. Experimental and theoretical results indicate that the doping of V species and the formation of heterostructures lead to charge redistribution. More importantly, the leaching of V species induces electron transfer form Co to O and then Ru through the Co-O-Ru electron bridge, optimizes the adsorption strength of the key intermediate, thereby reducing the free energy barrier of the rate-determining step and improving catalytic activity. This work proposes an effective strategy of using cation dissolution to induce electron transfer through the electron bridge and thus regulate the electronic structure of catalysts, providing new ideas for the design and development of efficient and stable electrocatalysts.

In the context of the global implementation of carbon neutrality goals and energy transformation, the task of developing sustainable new clean energy is urgent. Hydrogen, as a new type of energy with high energy density and zero carbon emissions, is considered a reasonable alternative to traditional fossil fuels [1]. As one of the most important green hydrogen production methods, electrolysis of water for hydrogen production has attracted attention from countries around the world [2]. The process of electrolyzing water involves two simultaneous reactions: the hydrogen evolution reaction (HER) at the cathode and the oxygen evolution reaction (OER) at the anode [3]. However, the slow multi electron transfer process in the anodic OER ($4OH^- \rightarrow O_2 + 2H_2O + 4e^-$, $E^\theta = 1.23$ V *vs.* RHE) and the high activation energy barrier required for water oxidation to form oxygen seriously hinder its industrial application [4,5]. Therefore, it is crucial to develop effective electrocatalysts to optimize electron transfer during the reaction process and lower the OER reaction energy barrier [6]. So far, the majority of electrolytic water catalysts used in industry are Ru-based and Ir-based materials [7,8], such as RuO_2 and IrO_2 are regarded as benchmark catalysts for OER, and Ru-based catalysts exhibit the best intrinsic OER activity (with an initial overpotential less than 200 mV). However, the high costs, scarcity and poor stability limit their further development and practical application [9–11]. Therefore, exploring and developing transition metal based electrocatalysts with reasonable prices and abundant reserves is currently a hot topic in the field of energy catalysis research [12,13].

In recent years, Co based catalysts have been widely studied in the fields of HER and OER due to their low cost and natural abundance [14]. Many types of Co based catalysts are gradually being explored and utilized, including oxides [15], hydroxides [16], nitrides [17], phosphates [18], sulfides [19], layered double hydroxides (LDH) [20]. Among them, Co oxides exhibit excellent electrochemical performance due to their unique electronic properties, variable chemical valence states and intrinsic OER catalytic activity. Co in its oxides has multiple oxidation valence states (such as Co^{2+} and Co^{3+}), and its ratio can be easily controlled and regulated. For example, Li *et al.* demonstrated the dual regulation of cation substitution and oxygen vacancy on ultra-thin Co_3O_4

* Corresponding author.
E-mail address: herx@swu.edu.cn (R. He).
[1] These authors contributed equally to this work.

https://doi.org/10.1016/j.cclet.2024.109793
1001-8417/

nanosheets resulted in excellent OER catalytic activity. The unique electronic state and ultra-thin structure ensure fast electron transfer and accessible customized active sites [21]. Lu's group [22] have been successfully prepared efficient OER electrocatalyst through electrospinning and carbonization processes. The Fe doped CoO/C nanofibers has faster charge transfer and reaction kinetics, exhibiting excellent OER activity and good cycling stability in alkaline electrolyte. In addition, numerous experiments have shown that the actual active species may differ from the initial ones. In the OER, most transition metal-based materials typically go through surface reconstruction process to generate truly active substances, which is an important step for enhancing electrocatalytic activity [23]. For Co-based catalysts, it has been confirmed that the dissolution or leaching of high valence metal ions can promote surface reconstruction or pre-activating of catalysts, thereby promoting the generation of actual active species CoOOH [24,25]. For example, Li's group [26] proved the dissolution of MoO_4^{2-} promotes surface reconstruction of $CoMoO_4$ to $Co_3O_4/CoMoO_4$ and $CoOOH/CoMoO_4$ heterostructures. After activation and surface reconstruction, partial electrons transfer from Co to Mo, making it easier to generate high valence Co species, which contributes to the superior OER activity. Fan *et al.* [27] induced the formation of high valent Co species on CoFeAl-LDH through a cationic leaching strategy. *In situ* Raman spectroscopy revealed that after CV activation to leach Al^{3+}, partial Co species in $CFA_{0.8}$-LDH/NF were reconstructed into high valence Co species CoO_2, which is the reason for the enhanced OER activity.

Based on the above ideas, we designed a vanadium doped heterogeneous catalyst. The designed catalyst Ru/V-CoO/CP was synthesized *in situ* on carbon paper (CP) by a simple strategy of hydrothermal followed by reduction. Fortunately, electrocatalysts exhibit excellent catalytic activity and stability in both HER and OER, achieving a current density of 10 mA/cm^2 with only 49 and 147 mV overpotentials in 1.0 mol/L KOH, respectively. The assembled electrolytic cell requires only 1.47 V to reach the same current density and can operate stably for 100 h. The XPS spectrum shows that the doping of V atoms has a synergistic effect with the formation of Ru/CoO heterostructures, which together promote electron transfer between metal atoms. Meanwhile, during the OER process, the dissolution of V can promote the transfer of electrons from Co to Ru through "Co-O-Ru" electron bridge, which facilitates the reconstruction of the catalyst to form the truly active species. Theoretical calculations further indicate that doping and interface engineering have optimized the electronic structure of Co, improved the energy level position of the d-band center, and facilitated the adsorption of intermediates, reduced the free energy barrier of the rate-determination step (RDS) ($O^* \rightarrow HOO^*$), thereby enhancing catalytic performance. This work provides new insights about the design of efficient electrocatalytic water decomposition through doping and interface engineering strategies.

The sample is synthesized through two steps. As shown in Fig. 1a, a certain amount of cobalt chloride, vanadium chloride, and ruthenium trichloride *in situ* growth on CP by the sample hydrothermal method to form the yellow precursor, then the precursor was transferred to a tube furnace for high-temperature annealing under the H_2/Ar atmosphere to obtain the final black sample. Fig. S1 (Supporting information) shows the optical images of bare CP, precursor/CP, and Ru/V-CoO/CP. The specific experimental details can be found in Supporting information. The surface morphology of the catalyst was analyzed through the scanning electron microscopy (SEM). It can be observed that the catalyst with or without the introduction of V exhibits a completely different morphology. The pure CoO sample exhibits a spherical morphology formed by stacking thick nanosheets (Fig. S2 in Supporting information), while the Ru/V-CoO, V-CoO and Ru/CoO follow the same morphology, exhibiting a nanoneedles grown on nanosheets (Figs. 1b and c, Figs. S3 and S4 in Supporting information). This change in morphology can increase the specific surface area of the catalyst, which is beneficial to expose more active sites for electrochemical water decomposition. The transmission electron microscope (TEM) was

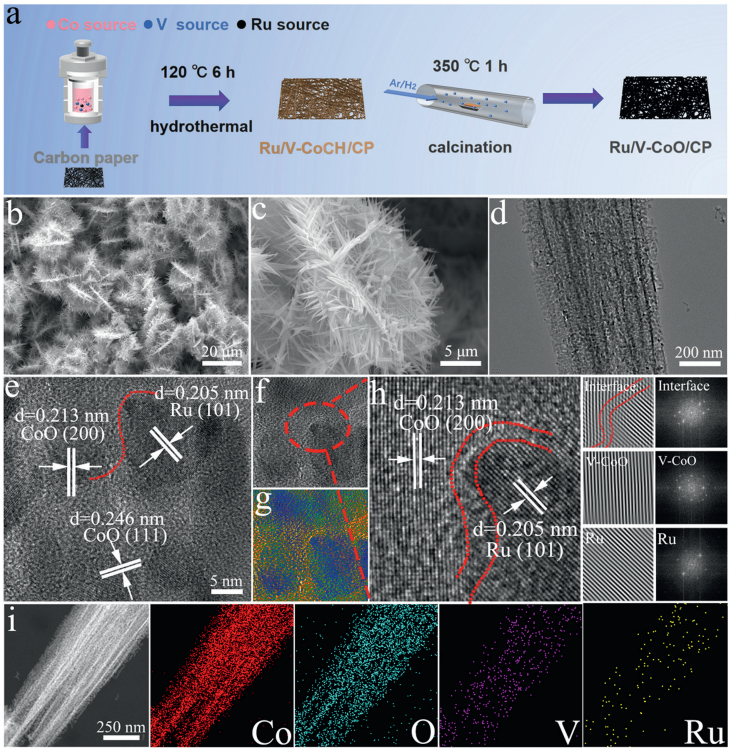

Fig. 1. (a) The synthesis diagram of Ru/V-CoO/CP. (b, c) SEM images of Ru/V-CoO. (d-h) TEM images of Ru/V-CoO. (i) EDX elemental mapping distribution diagram of Ru/V-CoO.

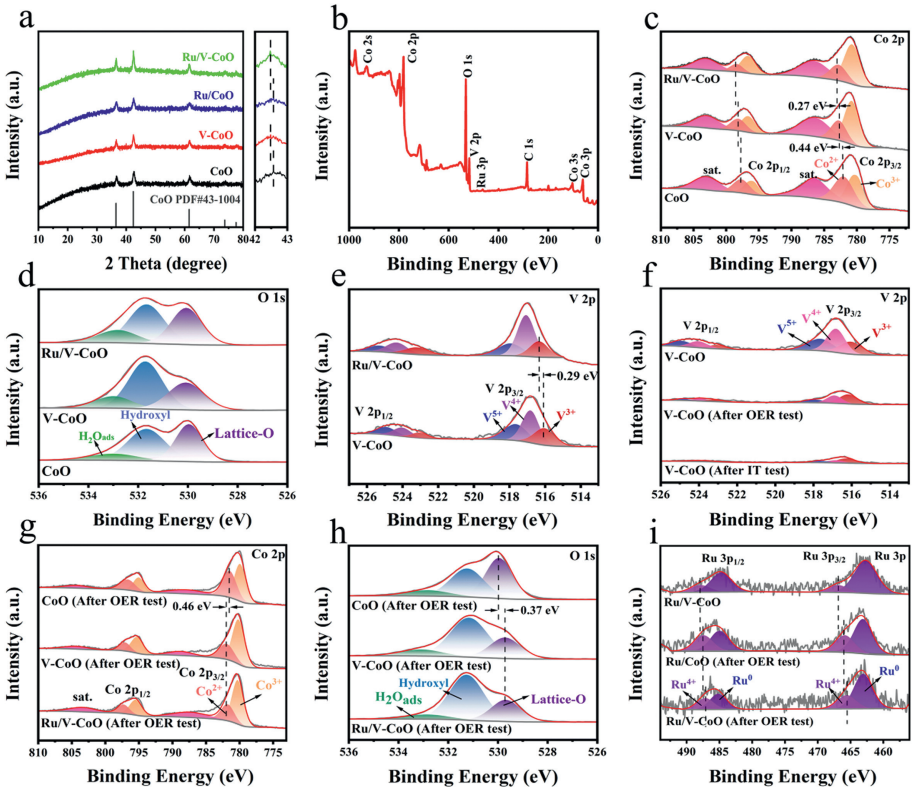

Fig. 2. (a) XRD patterns of Ru/V-CoO and other comparative samples. (b) XPS total spectra of Ru/V-CoO. (c, d) XPS spectra of Co 2p and O 1s in CoO, V-CoO and Ru/V-CoO. (e) XPS spectra of V 2p in V-CoO and Ru/V-CoO. XPS spectra of (f) V 2p, (g) Co 2p, (h) O 1s and (i) Ru 3p in various samples before and after OER testing.

used to study the more detailed microstructure of the catalyst and its nanoneedle structure was preliminarily demonstrated in Fig. 1d. As shown in Fig. 1e, the crystal plane spacing of 0.213, 0.246, and 0.205 nm correspond to the (200), (111) crystal plane of CoO and the (101) crystal plane of Ru, respectively [28,29]. A clearer heterogeneous interface can be observed by zooming in on the central region in Fig. 1f. Through Fourier transform, the clear and regular lattice fringes of CoO and Ru can be observed, and lattice distortion occurs at the interface (Figs. 1g and h). At the same time, through the selected area electron diffraction (SAED) pattern along the region axis, it can be observed that there are single crystal diffraction rings of CoO and Ru at the interface, which directly verifies the formation of heterostructures. The energy dispersive spectroscopy (EDS) mapping has provided evidence of a homogeneous dispersion of Co, O, V and Ru elements throughout the Ru/V-CoO (Fig. 1i), confirming the homogeneity of the sample. The above morphology and structural characterization clearly confirm the successful synthesis of Ru/V-CoO heterostructure catalysts.

As shown in Fig. 2a, the phase structure and crystallographic information of the different samples were analyzed by the X-ray diffractometer (XRD). The peaks at 36.5°, 42.4°, 61.5°, 73.7° and 77.6° correspond precisely to (111), (200), (220), (311) and (222) crystal planes of CoO (PDF#43-3004), respectively. Due to the slightly larger ion radius of V^{3+} compared to Co^{2+}, the introduction of V leads to lattice expansion, the diffraction peak between 42° to 43° degrees corresponding to the crystal plane (200) shifted slightly towards a small angle, which preliminarily proves the successful doping of V [30,31]. No relevant characteristic diffraction peaks of Ru and its compounds were detected, possibly due to the low content of Ru or its existence in a small size form [29,32]. The characteristic diffraction peaks of the precursor match well with CoCH (PDF #48-0083), which is consistent with most products obtained from similar hydrothermal reactions (Fig. S5 in Supporting information). The information about element composition and chemical state near the surface of materials were investigated by the X-ray photoelectron spectroscopy (XPS). Agreed with the element mapping results, the element of Co, O, V, and Ru were detected from the XPS spectrum in Fig. 2b, which further demonstrating the successful introduction of V and Ru. From Fig. 2c, it can be observed that the Co 2p spectrum of the sample shows four distinct peaks, including the peaks with binding energy at 781.1 and 796.9 eV belong to Co $2p_{3/2}$ and Co $2p_{1/2}$, respectively, and the peaks at 786.4 and 803.0 eV belong to the satellite peaks of Co [33,34]. The peaks situated at 532.82, 532.66 and 530.06 eV in the O 1s spectrum (Fig. 2d) correspond to adsorbed H_2O, hydroxyl (–OH) and lattice oxygen (M–O) on the catalyst surface, respectively [35]. The peak of Co^{2+} (782.52 eV) in V-CoO has a positive shift (0.44 eV) compared to the pristine CoO (782.08 eV), indicating that the doping of V affects the electron distribution around Co. After the introduction of Ru, the peak of Co^{2+} (782.79 eV) exhibits a further positive shift (0.27 eV) compared to V-CoO. Fig. 2e shows the XPS spectrum of V 2p, with three peaks located at 516.4, 517.1, and 517.9 eV corresponding to V^{3+}, V^{4+}, and V^{5+}, respectively [36,37]. The presence of V^{4+} and V^{5+} may be due to the oxidation of some V during the hydrothermal reactions or testing process [38]. Consistent with the situation of Co, the peak of V^{3+} has a positive shift after the formation of a heterostructure between V-CoO and Ru, indicating the existence of electron transfer between Ru and V-CoO, which also proved the formation of heterogeneous interfaces between Ru and V-CoO. To further explore the role of cationic V doping in OER process, we tested the XPS of the sample after OER for comparative analysis. Fig. 2f shows that the peak intensity of V species is significantly weakened after OER testing, indicating that the high valent V species on the surface of the sample are leached and dissolved in a 1.0 mol/L KOH solution. According to the ICP results, part of V in the catalyst dissolves

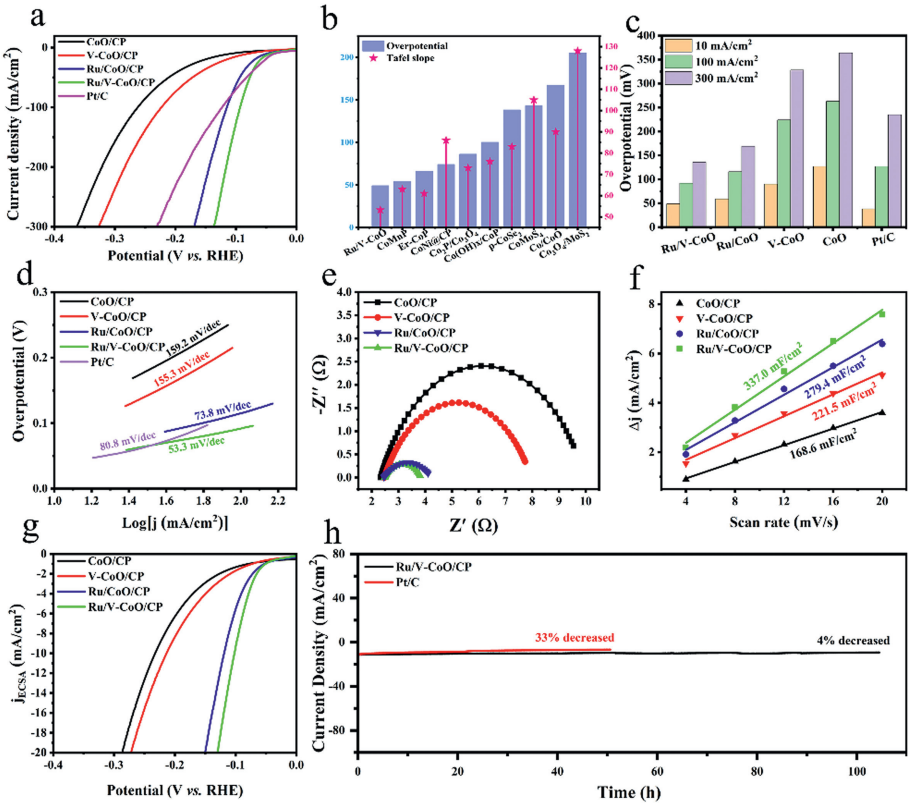

Fig. 3. (a) Polarization curves of all samples for HER. (b) Overpotential of all samples at different current densities. (c) Comparison with other works of HER performance. (d) Tafel slopes. (e) Nyquist plots. (f) The C_{dl} values obtained based on current density and scanning rates. (g) Normalized curves of HER. (h) Chronopotentiometry at 10 mA/cm^2 of Ru/V-CoO/CP.

rapidly at the beginning of OER testing and then tends to stability (Table S1 in Supporting information). Meanwhile, the weakening of the mapping signal of V species after OER testing also indicates the dissolution of V during the OER process (Fig. S6 in Supporting information) [38,39]. Compared to CoO, the diffraction peak of Co^{2+} in V-CoO and Ru/V-CoO shifts towards high binding energy by 0.46 eV after OER testing (Fig. 2g), while the diffraction peak of M-O and Ru^{4+} also shift towards low binding energy by 0.37 and 0.16 eV, respectively (Figs. 2h and i). In addition, the peak area ratios of $S_{M\text{-}O}/S_{M\text{-}OH}$ and $S_{Co^{3+}}/S_{Co^{2+}}$ (Fig. S7a in Supporting information) indicate that after OER testing, the catalyst surface with V doping has more oxides converted to hydroxyl oxides. The peaks situated at 485.5 and 463.1 eV in the Ru 3p spectra (Fig. 2i) correspond to Ru^0 on the catalyst surface [40]. The peak of Ru^{4+} shifts towards low binding energy, and the peak area of Ru^{4+} decreases compared to that of Ru/CoO after OER (Fig. S7b in Supporting information), proved that Ru gained electrons and maintained a low oxidation state during the reaction process. Therefore, it can be inferred that the change in binding energy should originate from the electron transfer from Co to O during the dissolution of V, and then oxygen further transfers electrons to Ru through the "Co-O-Ru" electron transport bridge. The main function of the "Co-O-Ru" electron bridge is to provide a pathway for electron transfer during the OER process. The dissolution of V enhances the ability of oxygen to receive electrons from Co and then transfer them to Ru, thereby promoting the reconstruction of the catalyst surface and boosting the stability of Ru.

The HER activity of Ru/V-CoO/CP and other control samples were evaluated by a standard three-electrode system under 1.0 mol/L KOH. The HER polarization curves of all samples and Pt/C are shown in Fig. 3a, and the prepared Ru/V-CoO/CP exhibits excellent activity with low overpotential of 49 mV to reach a current density of 10 mA/cm^2, which is almost equivalent to Pt/C (42 mV), far lower than Ru/CoO/CP (59 mV), V-CoO/CP (90 mV), CoO/CP (127 mV) and most recently reported catalysts (Fig. 3b and Table S2 in Supporting information). Fig. S8 (Supporting information) shows HER LSV curves of the Ru/V-CoO samples with different amount of Ru. Besides, Ru/V-CoO/CP required lower overpotential (92 and 136 mV) than the Pt/C electrode (127 and 235 mV) at large current density of 100 and 300 mA/cm^2 (Fig. 3c). The Tafel slope related to catalyst kinetics was calculated and obtained through LSV curves. As shown in Fig. 3d, compared with Ru/CoO/CP (73.8 mV/dec), V-CoO/CP (155.3 mV/dec), CoO/CP (159.2 mV/dec) and Pt/C (80.8 mV/dec), Ru/V-CoO/CP needs a smaller Tafel slope of 53.3 mV/dec, revealing Ru/V-CoO/CP has a faster kinetics behavior. In addition, the low Tafel slope of Ru/V-CoO/CP also reflects a conventional Volmer-Tafel mechanism, in which the rate-determining step (RDS) is associated with the H_2 desorption (Tafel step) [41]. In addition, the Nyquist plot (Fig. 3e) fitted based on the equivalent circuit diagram (Fig. S9 in Supporting information) is another key information for evaluating the kinetic behavior of catalysts. Obviously, Ru/V-CoO/CP possesses the smallest semicircle and the smallest charge transfer resistance (R_{ct}) of 1.7 Ω (Table S3 in Supporting information), which are lower than Ru/CoO/CP, V-CoO/CP and CoO/CP, indicates the Ru/V-CoO/CP has fast charge transfer capability and better electronic conductivity. The ECSA (Fig. S10 in Supporting information) obtained through cyclic voltammetry scanning in the Non-faradaic interval and the derived electrochemical double layer capacitance value (C_{dl}) (Fig. 3f) can provide a more intuitive understanding of catalytic activity [42]. Compared to Ru/CoO/CP (279.4 mF/cm^2), V-CoO/CP (221.5 mF/cm^2) and CoO/CP (168.6 mF/cm^2), Ru/V-CoO/CP (337.0 mF/cm^2) possesses largest C_{dl} value, indicating that Ru/V-CoO/CP has larger electrochemical specific surface area to expose more active sites.

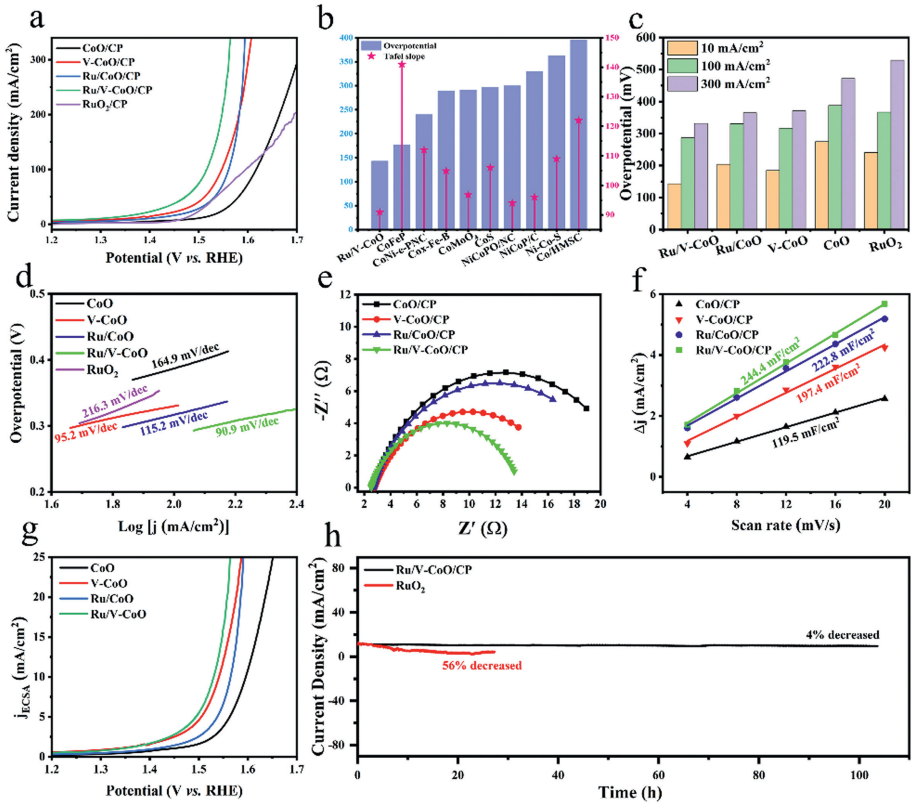

Fig. 4. (a) Polarization curves of all samples for OER. (b) Overpotential of all samples at different current densities. (c) Comparison with other works of OER performance. (d) Tafel slopes. (e) Nyquist plots. (f) The C_{dl} values obtained based on current density and scanning rates. (g) Normalized curves of OER. (h) Chronopotentiometry at 10 mA/cm^2 of Ru/V-CoO/CP.

This is consistent with the increase in active area caused by morphological changes observed in SEM. Furthermore, this also proves that the strategy of introducing Ru as the HER active site in the catalyst is effective. The HER normalized curve shown in Fig. 3g also confirmed that the Ru/V-CoO has greater intrinsic activity. Fig. 3h shows that the current density of Ru/V-CoO/CP only decreased by 4% after continuous testing for 100 h in 1.0 mol/L KOH, indicating its outstanding durability. As displayed in Fig. S11 (Supporting information), the overpotential of Ru/V-CoO at 10 mA/cm^2 only has a small increase of 8 mV, confirming that Ru/V-CoO has outstanding HER durability.

The OER performance of all samples were studied under the same conditions as HER. Similarly, Ru/V-CoO/CP exhibits outstanding OER performance with extremely low overpotential of 147 mV at 10 mA/cm^2, which is obviously better than Ru/CoO/CP (204 mV), V-CoO/CP (182 mV), CoO/CP (275 mV) and the commercial RuO_2/CP (256 mV) (Fig. 4a), and is also far superior to most recently reported cobalt based electrocatalysts (Fig. 4b and Table S4 in Supporting information). Ru/V-CoO/CP required lower overpotential than other comparative samples at current density of 100 and 300 mA/cm^2 (Fig. 4c). Fig. S12 (Supporting information) shows the OER LSV curves of V-CoO sample with different V doping amount. The Tafel slope of Ru/V-CoO/CP is 90.9 mV/dec (Fig. 4d), lower than Ru/CoO/CP (95.2 mV/dec), V-CoO/CP (115.2 mV/dec), CoO/CP (164.9 mV/dec) and RuO_2 (216.3 mV/dec), which indicates that both the doping of V and the introduction of Ru significantly improve the reaction kinetics of Ru/V-CoO/CP. Similarly, among all the samples, Ru/V-CoO/CP has the smallest R_{ct} value (11.3 Ω) (Fig. 4e and Table S5 in Supporting information) in OER, indicating its optimal conductivity, which facilitates charge transfer between the catalyst and electrolyte. The Nyquist plots and Bode-phase ones at different potentials further demonstrate that the V doping accelerates the kinetic of the catalyst (Fig. S13 in Supporting information). Meanwhile, the ECSA (Fig. S14 in Supporting information) and C_{dl} values indicate that the catalyst Ru/V-CoO (244.4 mF/cm^2) has a large electrochemical surface area to provide more active sites for OER (Fig. 4f). The normalized curve further confirms that Ru/V-CoO has better intrinsic activity without considering the influence of ECSA (Fig. 4g). The results of turnover frequency also demonstrate that Ru/V-CoO has excellent intrinsic activity (Fig. S15 and Table S7 in Supporting information). Fig. 4h displays that Ru/V-CoO/CP has excellent OER durability in 1.0 mol/L KOH, and only a small decay of 12 mV is presented after stability testing (Fig. S16 in Supporting information).

Considered its excellent performance in HER and OER, the Ru/V-CoO/CP was used as both cathode and anode to assemble an electrolytic cell for the overall water splitting (OWS), and the RuO_2||Pt/C cell was also assembled for comparison. The LSV curves in Fig. 5a showed that the Ru/V-CoO/CP||Ru/V-CoO/CP cell (Fig. 5b) only requires 1.47 V and 1.71 V to achieve the current densities of 10 and 350 mA/cm^2 in 1.0 mol/L KOH, which is lower than RuO_2||Pt/C cell (1.51 V and 1.76 V) and most recently reported catalysts (Fig. 5c and Table S6 in Supporting information). In addition, the assembled Ru/V-CoO/CP||Ru/V-CoO/CP cell ran stably for over 100 h at a current density of 10 mA/cm^2 without significant performance degradation, and the LSV curves match well with initial curves after 1000 CV cycles (Fig. S17 in Supporting information), which is far superior to commercial catalyst, demonstrating the great potential of this catalyst for application (Fig. 5d).

Density functional theory (DFT) calculations were employed to investigate the possible mechanism by which the introduction of V and Ru enhances the OER and HER catalytic activity. The theoretical models (Fig. S18 in Supporting information) of the samples (CoO, V-CoO, Ru/V-CoO) were constructed based on the TEM char-

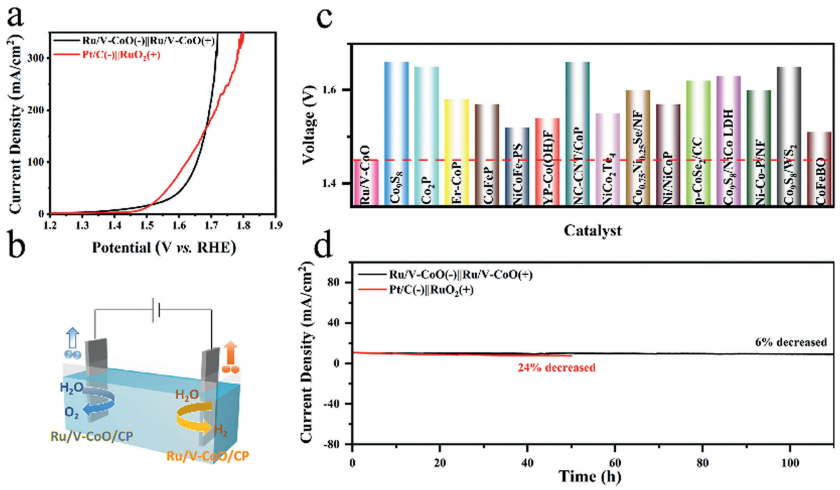

Fig. 5. (a) LSV curves of Ru/V-CoO||Ru/V-CoO and RuO_2||Pt/C for OWS. (b) Stability test of Ru/V-CoO||Ru/V-CoO and RuO_2||Pt/C for OWS. (c) Schematic diagrams of assembled electrolytic cell. (d) The performance comparison of Ru/V-CoO with the other works for OWS.

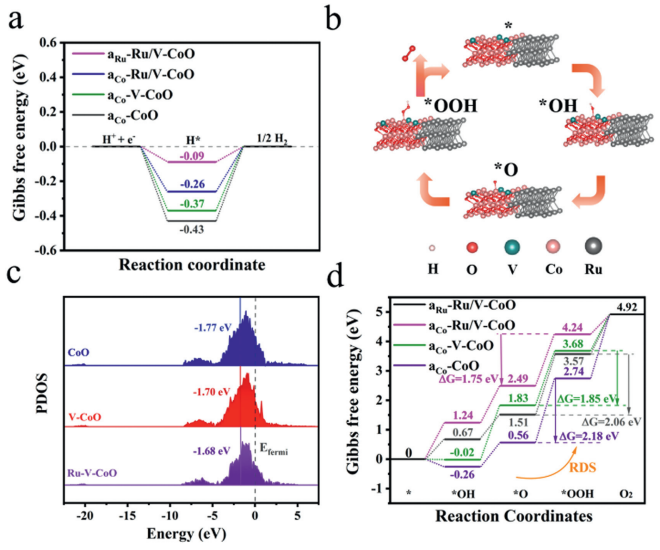

Fig. 6. (a) The HER Gibbs free energy diagram. (b) Schematic illustration of OER mechanism. (c) d-band centers. (d) The OER Gibbs free energy diagram.

acterization result, and then structural optimization was carried out (Fig. S19 in Supporting information). In order to further investigate the reasons for the improvement of HER/OER performance, the adsorption free energies of the intermediates in the HER/OER process were calculated on the optimized models, and the corresponding calculation models are shown in Figs. S20–S23 (Supporting information). In addition, the charge density difference was calculated to understand the electron transfer. As shown in Fig. S24 (Supporting information), the O and Ru atoms are in electron accumulation state (the yellow area), while Co is in an electron deficient state (the pale blue area), indicating electron transfers from Co to O and Ru. The HER activity can be reasonably described by the Gibbs free energy of the H* (ΔG_H, * is the active site) intermediate adsorbed on the catalyst surface. The adsorption free energy (ΔG_H) of ideal HER electrocatalyst should be zero or close to zero, which means that H* can easily adsorb and desorb on active sites in dynamic equilibrium [43–45]. Considering the significant increase in HER activity of the catalysts after introducing Ru, the ΔG_H on the Co and Ru sites were calculated separately (Fig. 6a). Compared to the pure CoO (−0.43 eV), both V-CoO (−0.37 eV) and Ru/V-CoO (−0.26 eV) exhibit H adsorption Gibbs free energy closer to 0 when Co as the active sites, indicating their superior HER activity. More importantly, the ΔG_H on the Ru site is closest to 0 (−0.09 eV), which suggests that the introduced Ru not only reduces the adsorption energy of H* by regulating the electronic structure of the catalyst, but also serves as an active site for HER, greatly enhancing the HER performance of Ru/V-CoO [46].

For OER (Fig. 6b), the projected density of state of Co 2p orbitals for each sample are shown in Fig. 6d. Evidently, the calculated positions of the d-band center [47,48] for CoO, V-CoO and Ru/V-CoO are −1.77, −1.70 and −1.68 eV, respectively. Compared with the pure CoO, the d-band center of Ru/V-CoO slightly shifts towards the Fermi level (0 eV), indicating an increase in the adsorption strength of the produced OER intermediates on the Ru/V-CoO surface after the introduction of V and Ru. A larger adsorption strength indicates a stronger electronic interaction between the intermediate and the catalyst surface, which is beneficial for the activation of the intermediates and thus promotes the improvement of catalytic performance (Note that the adsorption strength should not be too strong, otherwise the intermediates will be trapped in a deep potential well and difficult to carry out the subsequent reactions). The calculated results (Fig. 6d) shown that for all models, the Gibbs free energy change (ΔG) of the elementary reaction $O^* \rightarrow HOO^*$ is higher than those of the other elementary steps ($H_2O^* \rightarrow HO^*$, $HO^* \rightarrow O^*$, $HOO^* \rightarrow {}^*O_2$), illustrating that this step is the rate-determining step (RDS) of the OER process. The RDS free energy change (ΔG_{HOO^*}) of CoO is about 2.18 eV, while that of V-CoO, Ru/V-CoO (Co site) and Ru/V-CoO (Ru site) are 1.85, 1.75 and 2.06 eV, respectively. Obviously, the introduction of V and Ru atoms enhances the adsorption of water splitting intermediates on the catalyst surface by modulating the electronic structure of the catalyst, thereby reducing the free energy change of the RDS reaction and improving the OER activity. The theoretical results above are completely consistent with the experimental analysis.

In summary, the Ru/V-CoO/CP electrocatalysts with doping strategy and heterostructure has been fabricated by a simple two-step method for efficient electrocatalytic water splitting. The experimental characterizations confirmed that the leaching of V during OER can effectively induce electron transfer from Co to O and then to Ru through the electron bridge of “Co-O-Ru”, which promotes the evolution of Co into an active species while protecting Ru from excessive oxidation, thereby achieving efficient and stable HER and OER activity. As a result, the Ru/V-CoO/CP exhibits excellent bifunctional catalytic performance with overpotentials of 49

and 147 mV at a current density of 10 mA/cm^2 for HER and OER, respectively. The assembled Ru/V-CoO/CP||Ru/V-CoO/CP electrolytic cell can operate continuously for more than 100 h under a current density of 10 mA/cm^2 with a low voltage of only 1.47 V for overall water splitting. The DFT results suggest that the introduction of V and Ru regulates the electronic structure of Ru/V-CoO and shifts the d-band center upwards, thereby enhancing the adsorption strength of key intermediates and reducing the RDS free energy change; meanwhile, the introduced Ru also serves as the active sites for HER. These effects together improve the overall water splitting performance of the Ru/V-CoO/CP catalyst. The present work provides a deeper understanding of the roles of V doping in electrocatalytic water splitting, as well as new insights into the design of high-performance electrocatalysts.

Declaration of competing interests

The authors declare that they have no known competing financial interests or personal relationships that could have appeared to influence the work reported in this paper.

Acknowledgments

This work was supported by National Natural Science Foundation of China (No. 22006120), the Fundamental Research Funds for the Central Universities (No. SWU-XDJH202314), the Program for Innovation Team Building at Institutions of Higher Education in Chongqing (No. CXTDX201601011), Chongqing Municipal Natural Science Foundation (No. cstc2018jcyjAX0625).

Supplementary materials

Supplementary material associated with this article can be found, in the online version, at doi:10.1016/j.cclet.2024.109793.

References

[1] X. Liu, J. Meng, K. Ni, et al., Cell Rep. Phys. Sci. 1 (2020) 100241.
[2] S. Han, H.S. Park, J. Yoon, Chem. Eng. J. 477 (2023) 146713.
[3] H. Zhao, J. Yin, P. Xi, Trans. Tianjin Univ. 29 (2023) 395–405.
[4] Q. Niu, M. Yang, D. Luan, et al., Angew. Chem. Int. Ed. 61 (2022) e202213049.
[5] A. Majumdar, P. Dutta, A. Sikdar, et al., Small 19 (2023) 2207410.
[6] F. Chen, Z. Zhang, W. Liang, et al., Chin. Chem. Lett. 33 (2022) 1395–1402.
[7] X. Chu, L. Wang, J. Li, et al., Chem. Rec. 23 (2023) e202300013.
[8] G. Gao, Z. Sun, X. Chen, et al., Appl. Catal. B 343 (2024) 123584.
[9] J.J. Hou, J.T. Yuan, W. Zhang, et al., Green Energy Environ. 7 (2022) 432–439.
[10] J. Zhu, Z. Lyu, Z. Chen, et al., Chem. Mater. 31 (2019) 5867–5875.
[11] J. Zhu, M. Xie, Z. Chen, et al., Adv. Energy Mater. 10 (2020) 1904114.
[12] X. Wang, X. Xu, Y. Nie, et al., Adv. Sci. 10 (2023) 2301961.
[13] Y. Jiang, H. Liu, Y. Jiang, et al., Appl. Catal. B 324 (2023) 122294.
[14] X. Yu, Z. Pan, C. Pei, et al., Chin. Chem. Lett. 35 (2024) 108484.
[15] J. Zhang, J. Lian, Q. Jiang, et al., Chem. Eng. J. 439 (2022) 135634.
[16] X. Liao, T. Zhang, M. Dai, et al., J. Alloys Compd. 936 (2023) 168303.
[17] D. Guo, Z. Zeng, Z. Wan, et al., Adv. Funct. Mater. 31 (2021) 2101324.
[18] H. Li, Q. Li, P. Wen, et al., Adv. Mater. 35 (2023) 2302627.
[19] Y.R. Hong, S. Mhin, K.M. Kim, et al., J. Mater. Chem. A 7 (2019) 3592–3602.
[20] W. Liu, D. Zheng, T. Deng, et al., Angew. Chem. Int. Ed. 60 (2021) 10614–10619.
[21] Q. Wang, X. Xue, Y. Lei, et al., Small 16 (2020) 2001571.
[22] W. Li, M. Li, C. Wang, et al., Appl. Surf. Sci. 506 (2020) 144680.
[23] K. Fan, H. Zou, Y. Ding, et al., Small 18 (2022) 2107249.
[24] J. Chen, H. Li, S. Chen, et al., Adv. Energy Mater. 11 (2021) 2003412.
[25] Y. Zeng, M. Zhao, Z. Huang, et al., Adv. Energy Mater. 12 (2022) 2201713.
[26] L. Ge, W. Lai, Y. Deng, et al., Inorg. Chem. 61 (2022) 2619–2627.
[27] J. Zhong, Q. Chen, C. Guo, et al., Int. J. Hydrogen Energy 48 (2023) 23530–23539.
[28] J. He, F. Liu, Y. Chen, et al., Chem. Eng. J. 432 (2022) 134331.
[29] X. Chen, D. Shi, M. Bi, et al., J. Colloid Interface Sci. 652 (2023) 653–662.
[30] J. Liu, Y. Ji, J. Nai, et al., Energy Environ. Sci. 11 (2018) 1736–1741.
[31] M. Kuang, J. Zhang, D. Liu, et al., Adv. Energy Mater. 10 (2020) 2002215.
[32] L. Peng, L. Su, X. Yu, et al., Appl. Catal. B 308 (2022) 121229.
[33] T. Zhang, F. Song, Y. Wang, et al., Electrochim. Acta 404 (2022) 139648.
[34] J. Yao, M. Zhang, X. Ma, et al., J. Colloid Interface Sci. 607 (2022) 1343–1352.
[35] A. Moysiadou, S. Lee, C.S. Hsu, et al., J. Am. Chem. Soc. 142 (2020) 11901–11914.
[36] F.N.I. Sari, H.S. Chen, A.K. Anbalagan, et al., Chem. Eng. J. 438 (2022) 135515.
[37] X. Wang, Y. Zhou, J. Luo, et al., Electrochim. Acta 406 (2022) 139800.
[38] T. Zhao, X. Shen, Y. Wang, et al., Adv. Funct. Mater. 31 (2021) 2100614.
[39] H. Guo, L. Zhang, D. Ou, et al., Small 20 (2024) 2307069.
[40] L. Gao, X. Zhong, J. Chen, et al., Chin. Chem. Lett. 34 (2023) 108085.
[41] B.E. Conway, B.V. Tilak, Electrochim. Acta 47 (2002) 3571–3594.
[42] J. Zhang, R. Cui, X.A. Li, et al., J. Mater. Chem. A 5 (2017) 23536–23542.
[43] B. Yang, Y. Du, M. Shao, et al., J. Colloid Interface Sci. 616 (2022) 803–812.
[44] C. Pi, X. Li, X. Zhang, et al., Small 18 (2022) 2201137.
[45] Y. Wang, W. Qiu, E. Song, et al., Natl. Sci. Rev. 5 (2018) 327–341.
[46] T. Ling, S.Z. Qiao, Sci. Bull. 68 (2023) 2896–2897.
[47] J. Wu, Z.F. Wang, T. Guan, et al., Carbon Energy 5 (2023) e268.
[48] Q. Mao, W. Wang, K. Deng, et al., J. Energy Chem. 85 (2023) 58–66.